A. Fil, D. Moulton, B. Dudson, B. Lipschultz, K. Verhaegh, O. Février, O. Myatra, C. Theiler, M. Wensing, EUROfusion MST1 teams and the TCV team

On the effect of total flux expansion in TCV detachment and its modeling with SOLPS-ITER

On the effect of total flux expansion in TCV detachment and its modeling with SOLPS-ITER

A. Fil, D. Moulton, B. Dudson, B. Lipschultz, K. Verhaegh, O. Février, O. Myatra, C. Theiler, M. Wensing, EUROfusion MST1 teams and the TCV team

On the effect of total flux expansion in TCV detachment and its modeling with SOLPS-ITER

A. Fil*,[1,2] D. Moulton,[2] B. Dudson,[1] B. Lipschultz,[1] K. Verhaegh,[1,2] O. Février,[3] O. Myatra,[1] C. Theiler,[3] M. Wensing,[3] EUROfusion MST1 teams,[4] and the TCV team[5]

[1] *York Plasma Institute, University of York, Heslington, York, YO10 5DQ, UK*
[2] *Culham Centre for Fusion Energy, Culham Science Centre, Abingdon, OX14 3DB, UK*
[3] *Ecole Polytechnique Fédérale de Lausanne (EPFL), Swiss Plasma Center (SPC), CH-1015 Lausanne, Switzerland*
[4] *See the author list in "H. Meyer et al 2017 Nucl. Fusion 57 102014"*
[5] *See the author list of "S. Coda et al 2017 Nucl. Fusion 57 102011"*

Correspondence: *Alexandre Fil. Email: alexandre.fil@york.ac.uk, alexandre.fil@ukaea.uk

Abstract.

In ITER and DEMO, achieving detachment at lower densities might allow to reduce the amount of impurity seeded and to improve confinement by operating at lower separatrix densities. Analytic models predict that an increase of total flux expansion would allow such a reduction in the required upstream density for detachment. However, both experiments and modelling of TCV plasmas show the opposite trend. Using the 2D transport code SOLPS-ITER we model two density ramp discharges to understand the role of total flux expansion in TCV. The modeling demonstrates that this discrepancy with the expected effect of total flux expansion is due to enhanced neutral trapping in the low-R_t configuration compared to the high-R_t configuration, which counteracts the effect of total flux expansion, an effect similar to what was observed in DIII-D. By making magnetic and physical divertor configuration changes the expected effect of total flux expansion is recovered (and even exceeded), which shows the importance of the choice of baffling and divertor closure (angle between the divertor leg and the target) in achieving detachment at low density in current and future designs.

1   Introduction

Via a chain of atomic processes (ionization, recombination, charge-exchange, interaction with molecules, etc) at the edge of a tokamak plasma, a state of plasma detachment [1] [2] can be reached. It allows for dissipation

of most of the power in the Scrape-Off-Layer (SOL) and for reduction in the particle flux reaching the targets. For the range of midplane densities and power that ITER will be able to achieve (and to also avoid MARFE instabilities), it is currently foreseen that ITER will have to operate in such a regime [3] [4] for at least the first λ_q (from the separatrix to a few millimeters away). For future devices such as DEMO, the power crossing the separatrix will be even higher than in ITER [5] and the window for operating in detached conditions might be even further reduced, unless a solution can be found to obtain a detached plasma at lower midplane densities than with current divertor designs. In both ITER and DEMO impurity seeding will be needed, but achieving detachment at a lower threshold will still be useful as it might allow to seed less impurities and/or operate at lower separatrix density (thus improving confinement [6]).

A potential way of decreasing the detachment threshold (here defined as the upstream density at which the total ion flux to the target rolls-over) is to move the outer strike point(s) to a lower magnetic field (B) region (i.e. larger R_t) relative to the X-point, and adopt a configuration usually called "Super-X" [8]. The effect of total flux expansion f_R ($= \frac{Bu}{Bt} \approx \frac{Rt}{Ru}$, where "u" stands for "upstream" and "t" for "target") has already been investigated in simpler models, in particular in [7], [9] and [10], which showed that the target electron density and temperature scales approximately with f_R^2 and $1/f_R^2$, respectively, and that the target ion flux scales as $1/f_R$. Increasing total flux expansion (while keeping all other quantities constant) would then decrease the detachment density threshold.

SOLPS simulations in a "box" geometry [11] (i.e. 2D modeling box carefully designed to allow to change only the total flux expansion by rotating the box and increasing the radial position of the outer strike point) showed that total flux expansion significantly changes the plasma conditions at the target for fixed upstream conditions and that the upstream density threshold scale approximately as $1/f_R$, as predicted by the modified two-point model formulation (2PMF) presented in [7]. In realistic geometries, MAST-U [12] simulations with SOLPS have also shown the beneficial effect of total flux expansion [13] (higher target density, lower target temperature for "Super-X" simulations compared to "conventional" simulations), meaning that MAST-U would also detach at lower upstream density in the Super-X configuration.

However, UEDGE modeling [14] showed that for some configurations the total flux expansion had little effect on the detachment threshold. DIII-D experiments [7] also showed a weak impact of total flux expansion on target conditions and proposed that it was due to changes in the neutral trapping (i.e. the probability of neutrals to be ionized in the divertor region) between the different configurations, which could effectively counteract the effect of total flux expansion. Previous DIII-D modeling with SOLPS [7] was done for two of

those configurations at one density and while it showed the effect of neutral trapping on the target profiles, it did not discuss its impact on the detachment threshold. Recent TCV experiments [15] also found a lack of total flux expansion effect on the detachment density threshold.

In this paper, we use the 2D transport code SOLPS-ITER [16] [17] to model these TCV experiments, explain their results and give insight into the relative roles of total flux expansion and neutral trapping in the divertor. We start by presenting these experiments and their characteristics before moving to their modeling with SOLPS-ITER. In the last part of the paper, code experiments are designed to equalize neutral trapping between both configurations in order to recover the expected scaling of the detachment threshold with total flux expansion.

2   Total flux expansion effect on TCV detachment

2.1   Experimental total flux expansion scan in TCV

Recent experiments on the TCV tokamak [15] [18] have been conducted to investigate the effect of total flux expansion on detachment, especially its effect on the detachment density threshold. During these experiments, the midplane density was ramped up in 4 different configurations, with R_t (the R position of the outer strike point) ranging from 0.62 m to 1.06 m, a change in total flux expansion of ~ 1.7. Special care was taken to obtain similar upstream plasma conditions (including density, parallel connection length, input power and power crossing the separatrix).

The two best-diagnosed configurations, which we focus on for the rest of the paper, are shown on Figure 1. Both are ohmic L-mode plasmas with $I_p = 320\ kA, B_T = 1.42\ T$ in which the density was ramped up from $0.2n_G$ to $0.75n_G$ (where n_G is the Greenwald density). They correspond to an R_t of $\sim 0.68m$ (TCV pulse 52066, referred to as the "low-R_t" divertor configuration) and $\sim 0.92m$ (52064, referred to as the "high-R_t" configuration). The corresponding total flux expansion change is thus $0.92/0.68 \simeq 1.35$.

The peak (and total) ion current to the outer target is one of the main measurements used to determine if detachment occurs: it increases during the attached phase (pre-detachment) and then decreases ("roll-over") during detachment. It is measured with Langmuir probes [20] for the two cases in Figure 1.

The upstream density at which the target ion current starts decreasing (or again, roll-over) is designated as the detachment threshold. In Figure 2 we show the experimental variation of the peak ion current to the outer divertor. It gives similar results as plotting the total ion current to the target (as is also done in [15]) but is easier to compare to the simulations. The two R_t cases are quite similar, with the low-R_t case (52066)
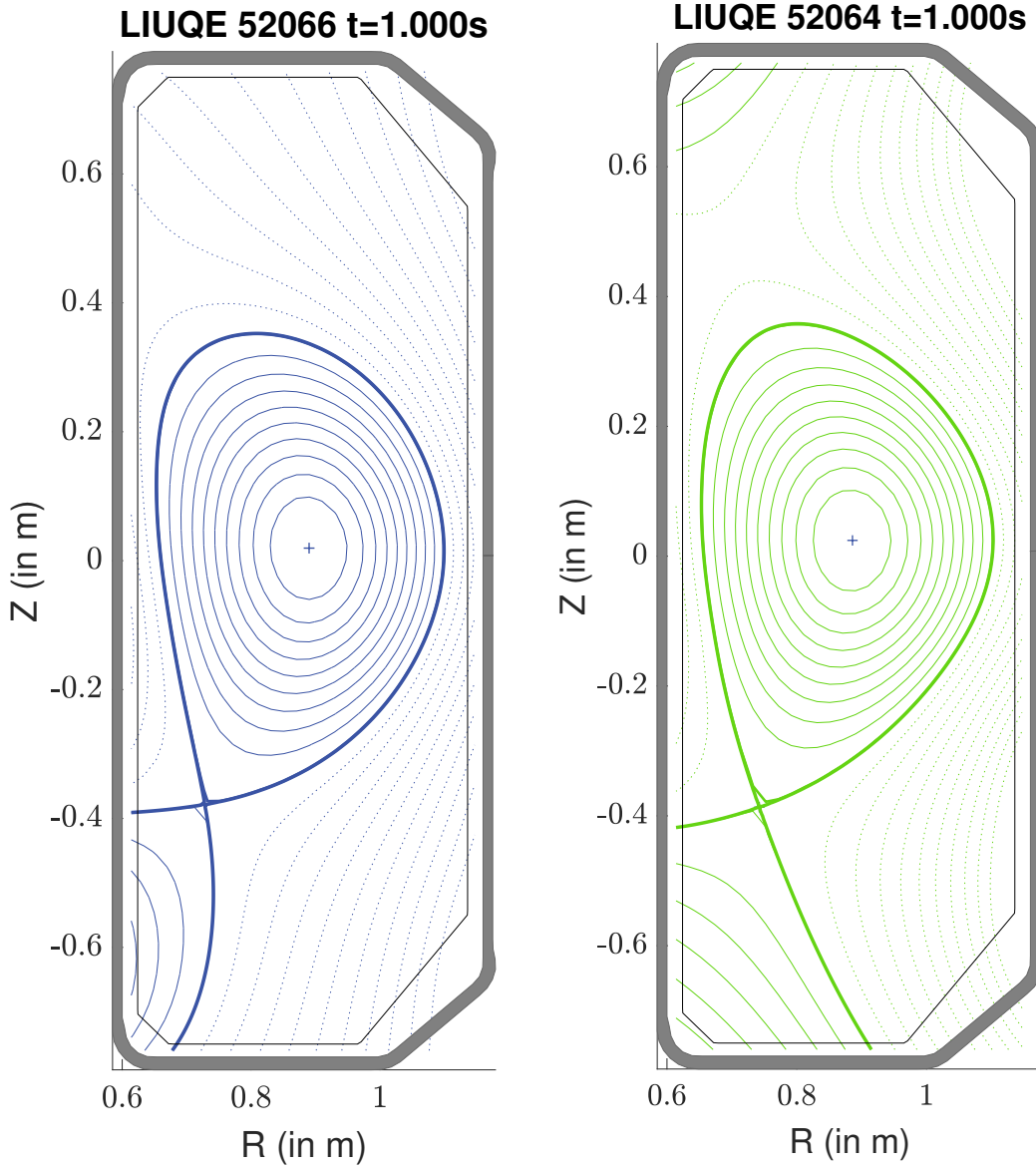
Figure 1: Equilibrium of two TCV shots with different total flux expansion: 52066 (low-R_t) and 52064 (high-R_t). Equilibrium reconstruction done with LIUQE [19] .

rolling over at a slightly lower upstream density than the high-R_t case (52064), while we would expect an increase of the detachment threshold by a factor of 1.35 from the high-R_t to the low-R_t case following the prediction based on the ratio of R_t.

The movement of the peak in the CIII emissivity profile (obtained from tomographic inversion of tangential CIII-filtered camera images of the divertor) is also commonly used at TCV as a precursor sign of detachment as well as a measure of the low-temperature region movement (ahead of the even lower-temperature ionization

front); in both configurations it was found to be very similar [15] [21]. Note that the two other configurations with even higher and lower R_t were not covered by the Langmuir probes but also showed a similar trend in the evolution of the CIII front [15]. Recent experiments seem to show that this lack of total flux expansion effect is still present in TCV H-mode plasmas [22].
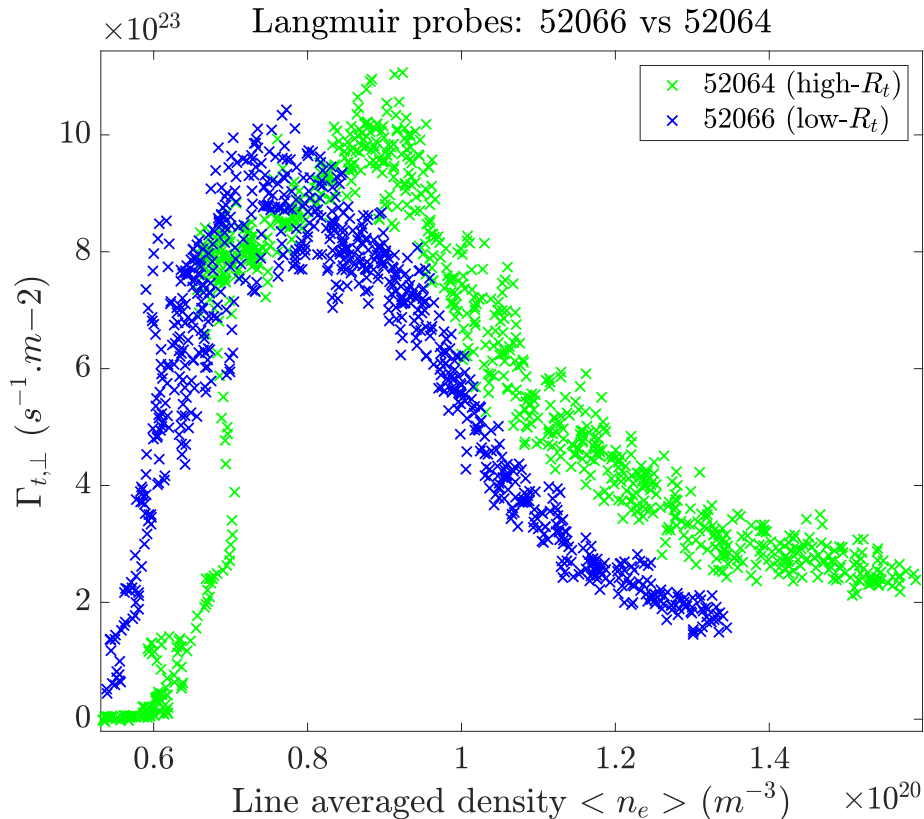
Figure 2: Evolution of the perpendicular ion flux to the outer target (for the probe where $\Gamma_{t,\perp}$ is peaked in attached conditions). Give similar results as plotting the total ion flux or the peak ion flux, as plotted in [15].

Even prior to detachment the TCV results contradict the prediction of theoretical models [9] and modeling work [11] described in the Introduction. Measurements of target electron density during the attached phase for both low-R_t and high-R_t configurations is indeed very similar. This again contradicts predictions that the high-R_t case should have higher density than the low-R_t case by a factor 1.35^2 for the same upstream conditions; this suggests the presence of additional effects (as concluded in [15]).

In the following, we model those two experimental shots with SOLPS-ITER in order to obtain a better understanding of these experimental observations. Our conclusion is that the variation in neutral trapping between these two configurations overcomes the effect of total flux expansion.

2.2   Modelling of a TCV total flux expansion scan with SOLPS-ITER

We use the 2D transport code SOLPS-ITER [16] [17] to model these two TCV experimental shots. SOLPS-ITER includes a combination of the fluid code B2.5 (see analysis grids in Fig. 3) as well as an EIRENE [23] Monte-Carlo kinetic neutrals grid that covers the plasma but also extends to surrounding walls.
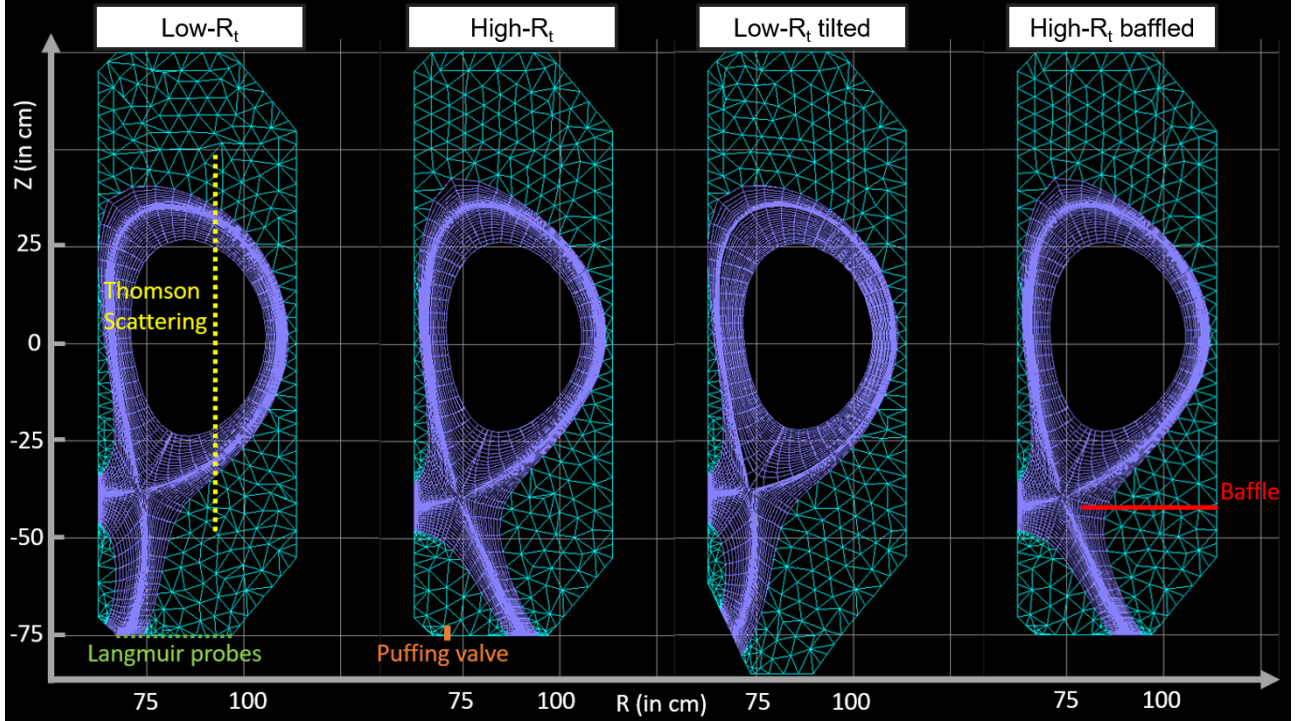
Figure 3: B2.5 plasma grids for the different simulations presented in this paper ("Low-R_t", "High-R_t", "Low-R_t tilted", "High-R_t baffled"). The EIRENE grids for kinetic neutrals extend towards the realistic TCV walls. The resolution of the B2 grids are 86x38 ($\parallel \times \perp$, aligned on flux surfaces with the lowest mesh spacing near the targets and the separatrix). Also shown is the position of the Thomson Scattering measurement ($R = 0.9m$), the Langmuir probes which cover the outer target, and the position of the gas valve from which we puff particles in the simulation.

We use an input power of $P = 600\ kW$ in these simulations, which is comparable to the power crossing the separatrix in those experiments (power loss measured by bolometry detector arrays, $P_{sep} \approx 400 - 600$ kW experimentally). In terms of pumping and puffing, we use an effective wall pump by choosing a recycling coefficient of 0.99 on all the wall surfaces and the targets. The combination of the puffing rate, the recycling coefficient and the Carbon chemical sputtering at the wall is chosen to match, within the error bars, experimental measurements from the CXRS [24] (for the observed carbon content), the Thomson Scattering (TS) system (for the upstream/midplane density and temperature profiles), the experimental puff rate range and the baratrons (neutral pressure). Radial transport is assumed to be diffusive and the transport coefficients are chosen to match experimental attached n_e (electron density) and T_e (electron temperature) profiles

at the midplane (shown in Figure 4, as measured by TS and the reciprocating Langmuir probe [25]). The transport coefficients are kept identical for all the simulations shown in this paper, with $D_\perp = 0.2 \ m^2.s^{-1}$, $\chi_{e,\perp} = \chi_{i,\perp} = 1 \ m^2.s^{-1}$.
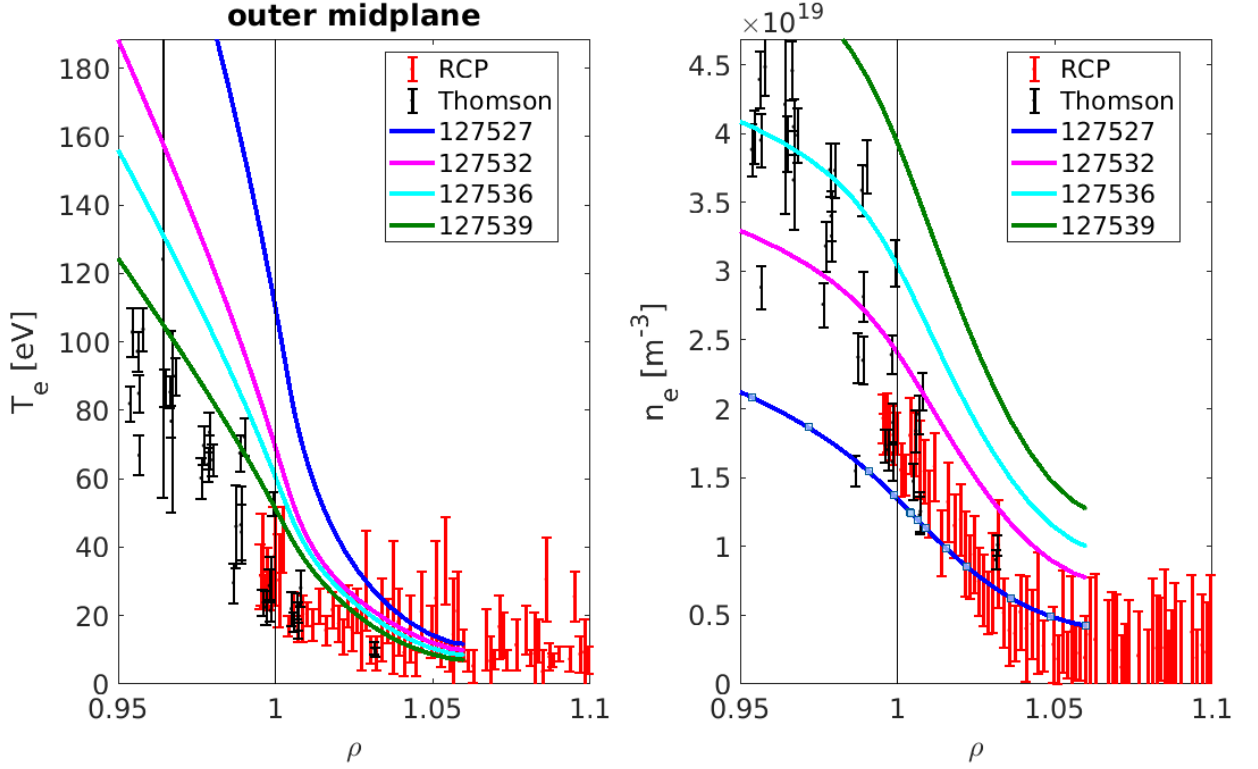
Figure 4: Comparison between experimental upstream n_e and T_e profiles from TS and RCP, and SOLPS-ITER profiles at different puff rates. The simulations outputs are stored on a MDS+ server and the numbers needed to access the data are indicated on the Figure.

Using those inputs, we perform multiple SOLPS-ITER simulations, each with a different puff rate. All the puffed particles enter the grid at the position of TCV valve 1 ($R = 0.69m$, $Z = -0.74m$). Each of these simulations converges in about 10000 time steps of 10^{-5} s. Those steady state simulations are deemed to be converged when all quantities are constant with time and that the puffed neutral flux is equal to the pumped neutral flux ($\Gamma_{puffed} = \Gamma_{pumped}$). The range of upstream densities obtained in this set of simulations is $0.8 - 7 \cdot 10^{19} \ m^{-3}$ and covers the range of upstream densities observed during experimental density ramps (actually even exceed it). Note that the puff rates are very similar to the experimental rates ($0.2 - 2.4 \cdot 10^{21}$ particles/s). As we increase the puff rate and thus the upstream density, simulations progressively reach a detached regime characterized by the rollover of the ion flux at the targets and very low target T_e.

In figure 5, the flux tube particle balance for the low-R_t configuration is plotted, from the entrance of the

divertor to the outer target. In this plot, we have $\Gamma_{target} = \Gamma_{up} + S_{ionization} + S_{recombination} + \Gamma_{Rad.transp.}$, where Γ_{target} is the ion flux to the outer target (at the end of the flux tube), Γ_{up} is the ion flux entering the flux tube (around the X-point) and is mainly caused by ionization upstream, $S_{ionization}$ and $S_{recombination}$ are respectively the total ionization and the total recombination sources in the flux tube (so negative for the recombination as it is a sink of particles), and $\Gamma_{Rad.transp.}$ is the net radial flux of particles (positive if more particles are entering than leaving the domain, negative otherwise).

We observe that recombination is not a strong contributor to the rollover of the target ion flux at detachment, consistent with TCV experimental measurements by Verhaegh [26] and previous modelling of TCV [27]. The consistency with experimental measurements is also true for the ion source (S_{ion}) which is the source of most of the ion target current; both the ion source and the target ion flux roll-over as the upstream density is increased. From previous modeling and experiment we know that the ion source is limited by the power available for ionization [26] [27].

Consistent with experiments [15], the simulated target profiles in attached conditions do not follow the predicted effect of total flux expansion. The expected target density, temperature and ion flux for the high-R_t configuration and the simulated ones are shown in figure 6. The "expected" high-R_t target quantities are calculated as if total flux expansion was the only change between the two configurations, i.e. $(\Gamma_{target})_{expected} = (\Gamma_{target})_{low-R_t} \times (f_R)_{high-R_t}/(f_R)_{low-R_t}$, $(T_{target})_{expected} = (T_{target})_{low-R_t} \times ((f_R)_{low-R_t}/(f_R)_{high-R_t})^2$ and $(n_{target})_{expected} = (n_{target})_{low-R_t} \times ((f_R)_{high-R_t}/(f_R)_{low-R_t})^2$, according to equation (1). Both configurations are attached with similar upstream profiles. The large discrepancy observed in the target profiles suggests that an additional effect is counteracting the effect of total flux expansion in those simulations and in the experiments.

Prior to the target ion flux rollover, we observe that the CIII emissivity peak detaches from the target as observed experimentally. It is found in the simulations that the radiation from CIII contributes to most of the total impurity radiation and thus that tracking the total impurity radiation front gives almost identical results as tracking the CIII radiation front. Moreover, the ionization region also detaches from the target, as can be seen on Figure 8.

These results are consistent with experimental observations [15] [21] of the dynamic of the ionization and recombination regions using the DSS (Divertor Spectroscopy) [26]. The target density roll-over occurs at higher upstream density than the ion flux roll-over and the density peak stays very close to the targets. The
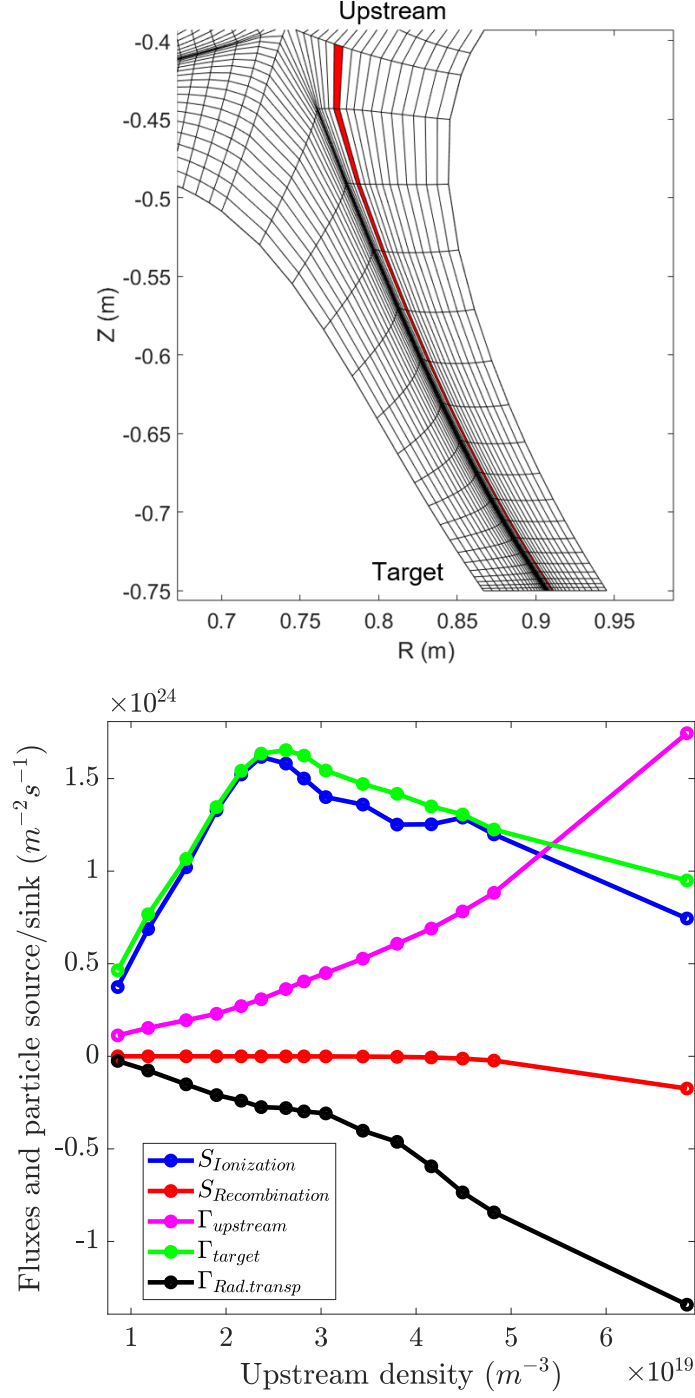
Figure 5: Left: Flux tube (red domain) for which the ion flux to the target is peaked in attached conditions. In the rest of the paper we will refer to this flux tube (and its equivalent for the low-R_t configuration) when doing particle balances and plotting the ion flux. Right: Flux tube particle balance for all the high-R_t cases. Γ_{target} is the ion flux to the outer target, Γ_{up} is the ion flux entering the divertor and is mainly caused by ionization upstream, $S_{ionization}$ and $S_{recombination}$ are respectively the total ionization source and the total recombination sink in the divertor, and $\Gamma_{Rad.transp.}$ is the net radial flux of particles out of the flux tube. The rollover of Γ_t occurs for $n_{e_{up}} \approx 3.10^{19} m^{-3}$.

density peak starts dropping when recombination becomes non-negligible, for the simulation with the highest

puffing rate (i.e. $n_{e_{up}} \sim 7 \cdot 10^{19} m^{-3}$).
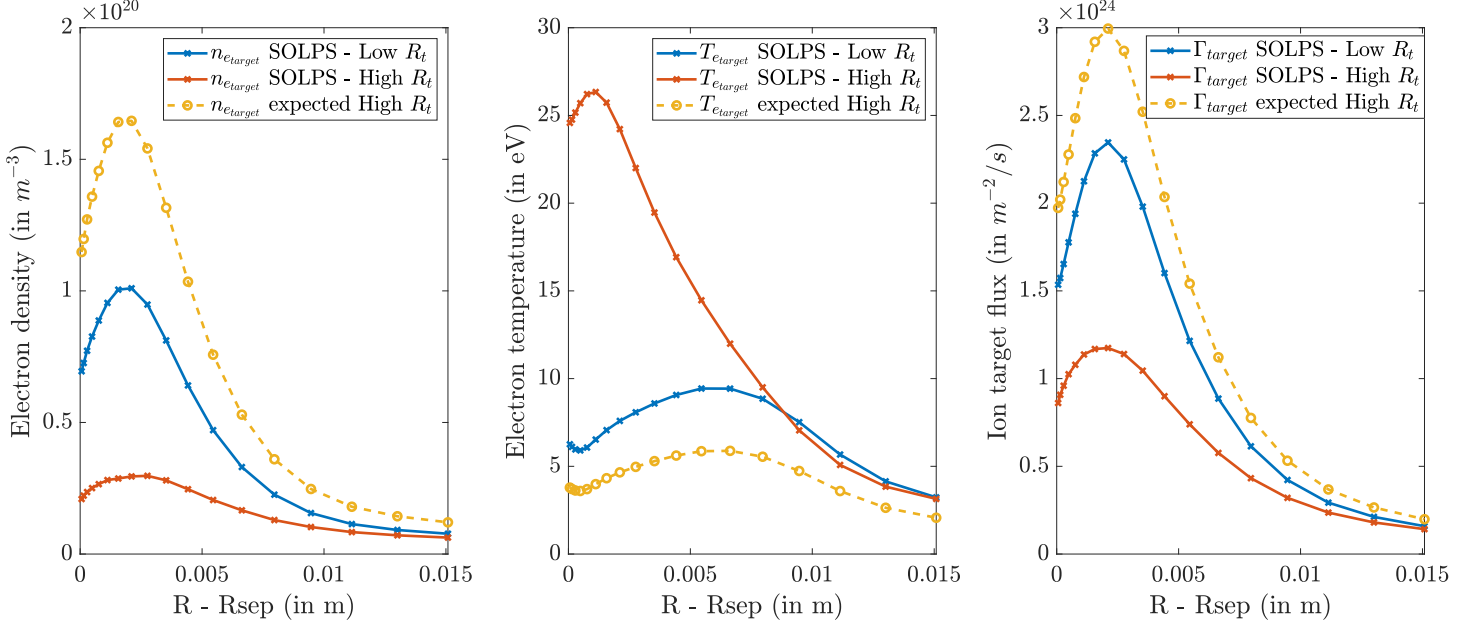
Figure 6: Target profiles of the electron density, the electron temperature and the ion flux. Both configurations are attached and with almost identical upstream profiles. Also showed is the expected target profiles of the high-R_t configuration if total flux expansion was the only factor changing in equation (1) (Modified 2-point model formulation equations for the target density, temperature and Γ_t).
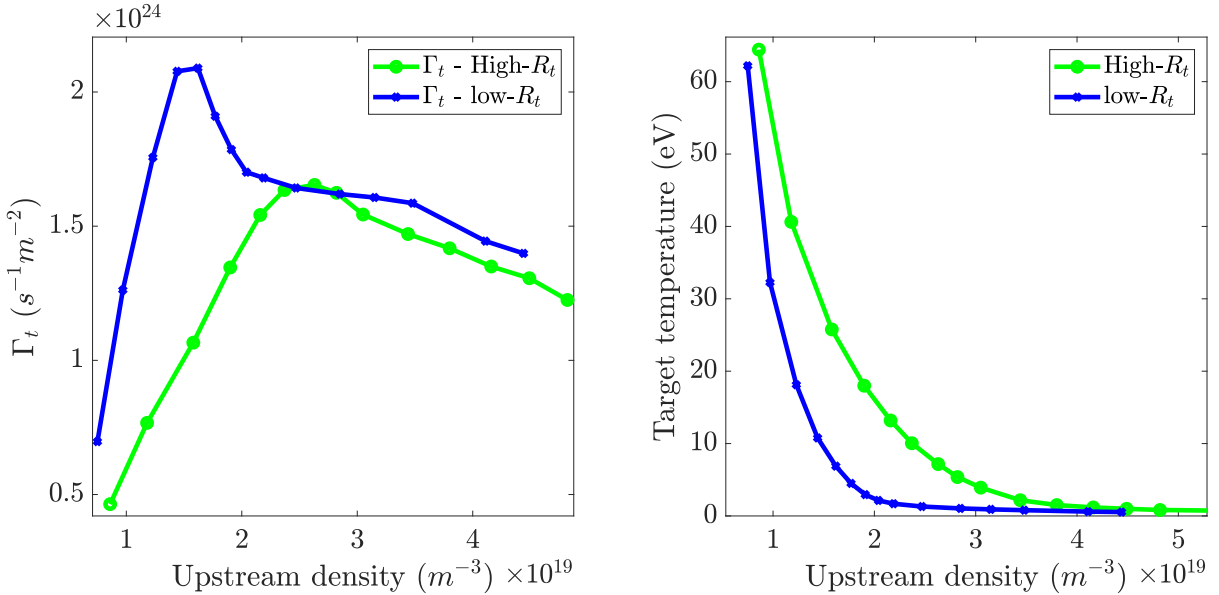
Figure 7: Evolution of the ion flux to the outer target and the target electron temperature of the flux tube where the peak Γ_t is in attached conditions, for the low-R_t and high-R_t configurations.

The target ion current roll-over, which occurs at different upstream densities for the low-R_t and high-R_t configurations, implies that detachment starts at a lower upstream density for the low-R_t compared to the high-R_t case (Figure 7). The earlier detachment threshold for the low-R_t case is also reflected in the right plot

of Figure 7, where we observe that the low-R_t case target temperature drops faster as a function of upstream density than for the high-R_t case. Following the total impurity radiation front, similarly to what is done experimentally using bolometry [15], also clearly shows an earlier detachment for the low-R_t configuration (see Figure 8). All of those observations give a $N_{thres} = (n_{thres})_{low-R_t}/(n_{thres})_{high-R_t}$ of $\simeq 0.81$ (ratio of detachment thresholds between low-R_t and high-R_t configurations) instead of the predicted total flux expansion scaling of 1.35.
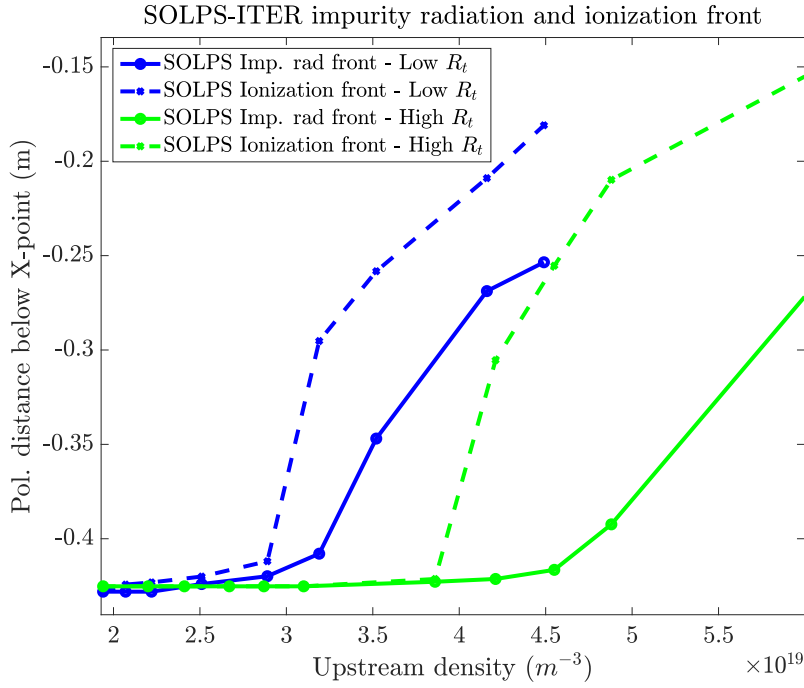
Figure 8: Evolution of the impurity radiation front with increasing upstream density for the two configurations. The radiation front position is calculated with the same method as in the experiments.

The uncertainties of the experimental measurements (and thus the comparison) remains large for the profiles of ionization source, recombination sink or the estimation of the upstream density. The former prevents from having a clear comparison with experiments (for example by combining Figure 2 and 7). With the diffusivities used in this paper, it seems that the target ion flux is overestimated by a factor $1.5 - 2$, as can be seen on Figure 9 and when comparing Figure 2 and Figure 7. This overestimation occurs for both low-R_t and high-R_t configurations.

A better match to the upstream and target profiles was obtained by increasing $D_\perp$ from 0.2 $m^2.s^{-1}$ (as for the cases shown in this paper) to 2 $m^2.s^{-1}$, thus increasing radial transport in the outer divertor domain and reducing the target ion flux to values similar to experimental ones. However, this improved agreement
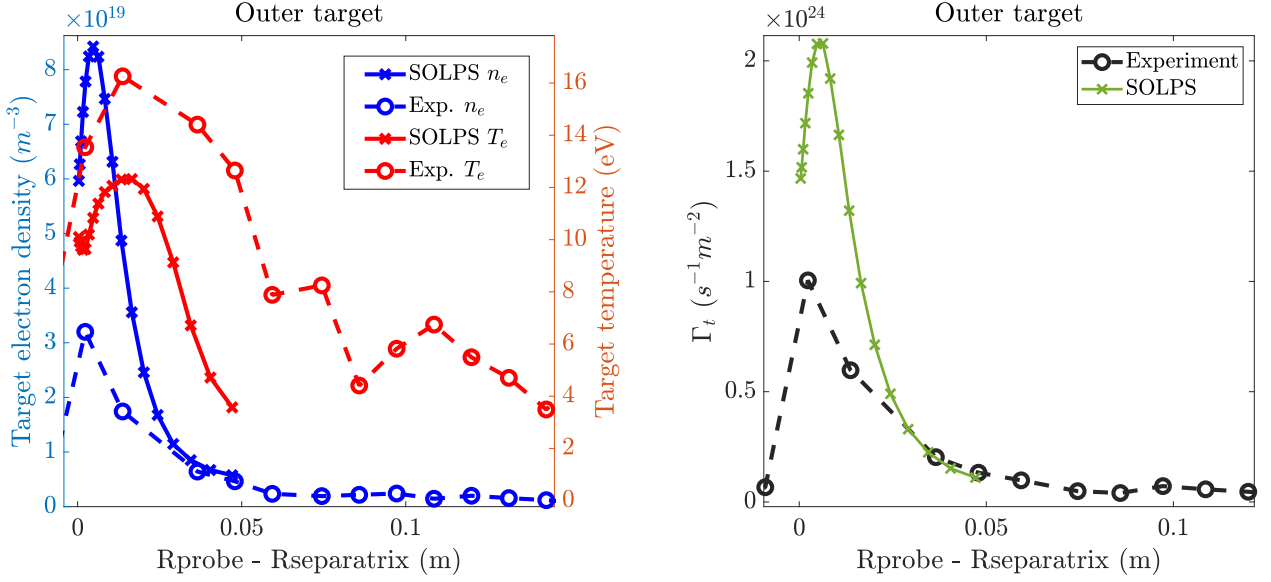
Figure 9: Comparison between experimental target j_{sat}, n_e and T_e profiles from Langmuir probes and SOLPS-ITER outputs, in attached conditions.

came at the cost of an implausibly high electron temperature at rollover of 10 eV, compared to $1-2$ eV for the simulations with $D_\perp = 0.2 \ m^2.s^{-1}$. This high rollover temperature is due to the very high radial flux of particles out of the simulation domain. One important point is that such a diffusivity increase does not drastically change the ratio of density threshold between configurations ($N_{thres} = 0.76$ instead of 0.81). The qualitative results and the conclusions of the paper does not depend on this choice of diffusivities, at least for the three different diffusivities tested (a density scan with $D_\perp = 1 \ m^2.s^{-1}$ was also performed but not shown in this paper). The agreement at the inner target is poor, as in [27], and we believe that to enhance both the outer and inner divertor agreement would require SOLPS-ITER simulations to be run with drifts and ballooning-like diffusivities, the former of which was challenging and unsuccessful so far. The inclusion of poloidally-varying diffusivities ($= D_\perp \times B^2$) was tried and was not, by itself, enough to recover the inner-outer asymmetry. The next section will focus on the potential counteracting effects of total flux expansion via analysis of the simulations and code experiments.

3   Effect of neutral trapping on the total flux expansion scan

3.1   Mechanisms which counteract the effect of total flux expansion

We have used the modified 2 point model formulation (2PMF) equations [7] [28] to analyze the differences between the high-R_t and the low-R_t divertor in the development of detachment and thus delineate the various

effects that may be affecting the detachment threshold beyond the effect of total flux expansion. Equation (1) is the 2PMF equation for Γ_{tgt}, the ion flux to the target, where γ_{sheath} is the sheath heat transmission coefficient, m_D is the mass of Deuterium, p_{tot_u} is the total upstream pressure, q_u is the upstream heat flux, M_t is the target Mach number, f_{mom}/f_{pwr} are the fraction of momentum/power lost between upstream and the target and R is the radial position (upstream and at the target). The overall prediction of the target ion flux is extremely close to the direct code output for Γ_t (1% difference, not shown).

$$\Gamma_{tgt} = \left[\frac{\gamma_{sheath}}{8 \cdot m_D}\right] \cdot \left[\frac{p_{tot_u}^2}{q_u}\right] \cdot \left[\frac{2}{p_{KR_{tar}}}\right] \cdot \left[\frac{4 \cdot M_t^2}{(1 + M_t^2)^2}\right] \cdot \left[\frac{(1 - f_{mom})^2}{(1 - f_{pwr})}\right] \cdot \left[\left(\frac{R_t}{R_u}\right)\right] \tag{1}$$

Comparing the ratio of the factors surrounded by square brackets in equation 1 for the high-R_t and low-R_t cases shows that most of the terms of equation 1 are similar between configurations when cases with similar upstream conditions are compared (same $n_{e_{up}}$ in both low-R_t and high-R_t). The exceptions are the total flux expansion term $(\frac{R_t}{R_u}) = f_R$ and the power and momentum losses term $\frac{(1 - f_{mom})^2}{(1 - f_{pwr})}$. Going a step further and decomposing the different power sources and sinks in the code, we find that the main difference between the power losses in the high-R_t configuration and the low-R_t configuration is caused by impurity radiation, hydrogenic radiation (due to higher ionization) and radial transport terms. Interestingly, when density scan simulations are performed without Carbon (so no power sink from impurity radiation), the low-R_t case still detaches before the high-R_t case (both at higher upstream densities than their equivalent cases with Carbon) and the difference in power losses is now a difference due hydrogenic radiation only, which points to an increased ionization in the low-R_t case compared to the high-R_t case. The increased power losses in the low-R_t configuration are correlated with a higher neutral content in the divertor compared to the high-R_t configuration, and all those observations support an increased neutral trapping in the low-R_t case than in the high-R_t.

One illustration of that is presented in Figure 10, which represents the fraction of neutrals created on the outer target which are being ionized in the flux tube where Γ_t is maximal in attached conditions (same flux tube as in Figure 5 and 7). We indeed observe a larger fraction (i.e. higher neutral trapping) in the low-R_t case, which then decreases in both configurations as they detach and as the divertor ionization source decreases (see Figure 5).

We note that there are several differences between the neutral pathways between the two divertors which could explain this difference in neutral trapping:

- The low-R_t case strike point is located near the inner wall which will help confine neutrals near the target.

- The poloidal angle of incidence would tend to direct recycling (and reflected) neutrals more towards the private flux region as opposed to the high-R_t case where the separatrix poloidal angle of incidence would tend to direct recycled (and reflected) neutrals into the main SOL.

When neutrals are directed towards the main SOL they are much less likely to return to the strike point region and be ionized (which would increase the density and drop the temperature and shift the divertor closer to detachment). This effect has already been studied and has been found to explain the lower detachment threshold for "vertical-target" vs "horizontal-target" divertors [29]. To confirm these observations, we now present "experiments in the code" to modify the neutral trapping properties of the two divertor configurations.
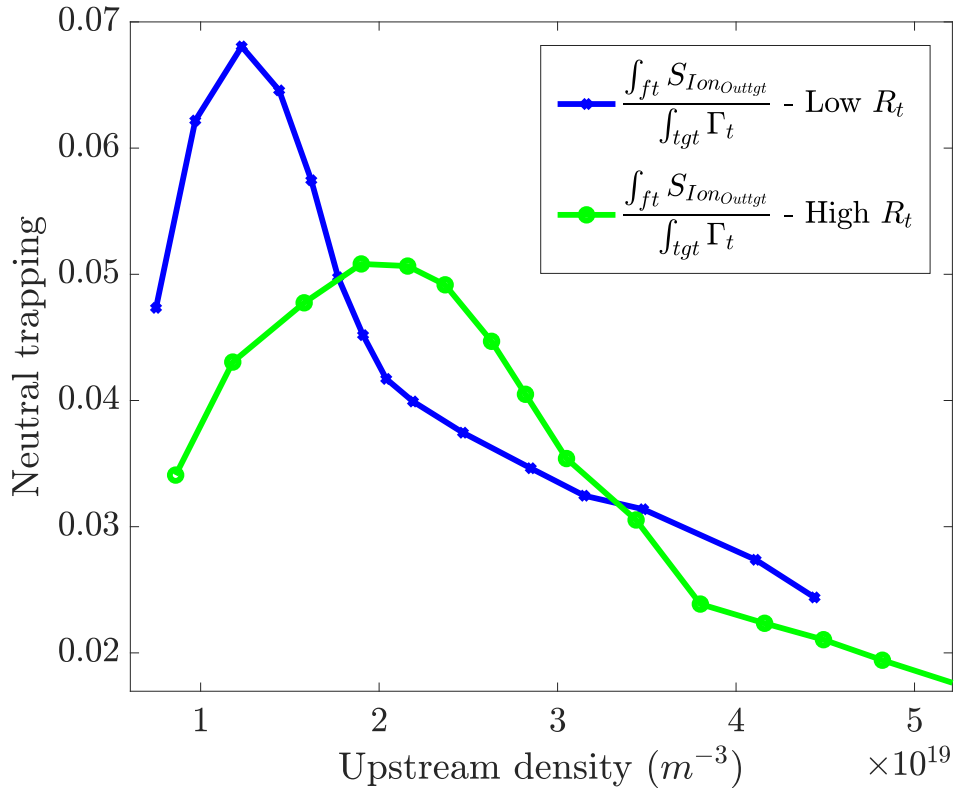
Figure 10: Measure of the neutral trapping as the fraction of neutrals which ionize in the flux tube (and not in the upstream SOL, in the core, in the Private Flux Region (PFR) or in the inner divertor). To calculate this quantity, we use the integrated ionization source in the flux tube, but only from neutrals which are created at the outer target. We then divide this quantity by the total target ion flux.

3.2   Effect of strike point angle on neutral trapping and TCV detachment

To investigate the second bullet outlined above, we have modified the low-R_t case such that the angle between the outer divertor leg and the wall is now exactly the same as in the high-R_t case, which should raise the detachment threshold. This was achieved by tilting the existing TCV wall, as shown in the third plot of Figure 3.

Instead of being recycled towards a region close to the separatrix as in the low-R_t case, the neutrals are now mainly recycled towards the far SOL and in a more open region. In the following, we designate this configuration as "Low-R_t tilted". Simulations of a density scan in this configuration is as expected: detachment occurs at a higher upstream density threshold than the normal low-R_t scan, and slightly higher than in the high-R_t configuration, as is shown on Figure 11. In terms of the ratio of upstream density at rollover, N_{thres}, we are now at $\simeq 1$ (Low-R_t tilted vs. High-R_t) instead of 0.81 (Low-R_t vs. High-R_t) and we are thus closer to the predicted scaling for the effect of total flux expansion only (i.e. 1.35).
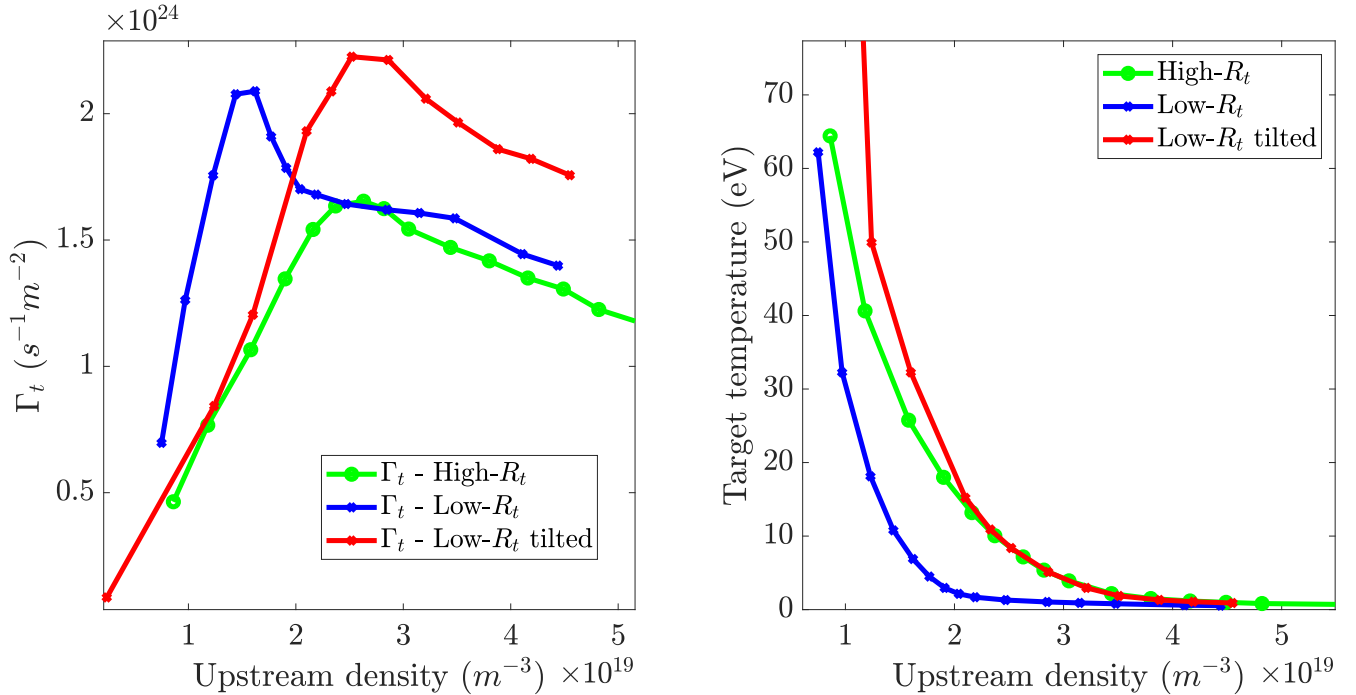
Figure 11: Evolution of the ion flux to the outer target and the target electron temperature of the flux tube where the peak Γ_t is, for the Low-R_t, High-R_t and Low-R_t tilted configurations.

Changing the divertor closure by using the same incidence angle for both configurations thus allows to partially recover the total flux expansion effect on TCV.

3.3   Effect of complete divertor neutral baffling on TCV detachment

Our second modification of the neutral trapping addresses the first cause outlined above - the goal is to make the neutral trapping in the divertor more uniform between configurations. We thus add a baffle-like structure as shown on the right plot of Fig. 3 which strongly limits the ability of neutrals to escape to the SOL above the X-point; it does not change the escape probability to the region around the X-point for each configuration. Note here that the baffle acts only on the neutrals, not on the plasma. This effect would be strongest for the high-R_t case given that the neutrals in the low-R_t configuration tend to be trapped between the separatrix and the inner wall - in the private flux region.

The comparison of the low-R_t and high-R_t configurations for a density scan was again performed (with baffles in both configurations). A large increase of the neutral content in the divertor for the same upstream densities is observed, as puffing must be increased for a given upstream density. This is due to the fact that the gas puffing slot is in the bottom part of TCV and that the baffle-like structure is preventing injected molecules from reaching the midplane and increasing density there (by dissociation and ionization of the created neutrals).

This additional structure also considerably closes the divertor and thus increases the neutral trapping, as can be seen on Figure 12, where the neutral trapping is significantly increased in the baffled cases compared to the non-baffled cases. Figure 12 also shows that there is a larger increase in the high-R_t configuration than in the low-R_t configuration which tends to homogenize the neutral trapping between the two configurations. This results in both configurations rolling over at lower upstream densities, as can be seen on Figure 13 (for example, the detachment threshold of the high-R_t case is $\simeq 1.7 \times 10^{19} m^{-3}$ lower with the baffle, similarly to what is found in recent modeling of the TCV baffle upgrade [30]). As the high-R_t configuration is more affected by the baffling than the low-R_t configuration, its target flux now rolls-over at lower upstream density than the low-R_t baffled case. However, the baffle itself does not allow to fully recover the expected N_{thres} (1.07 instead of 1.35). Only the combination of baffling and changing of the incidence angle finally allow to recover a significant observable effect of total flux expansion on the detachment threshold, and even exceed it, as can be seen on Figure 13 (red curve vs. green have a $N_{thres} \simeq 1.52$). Note that the target profiles in attached conditions (as shown in Figure 6 for the cases without baffle) are consistent with this, with a significantly higher target density in the high-R_t baffled configuration (i.e. much lower target temperature) than in the low-R_t tilted baffled configuration, for similar upstream conditions.
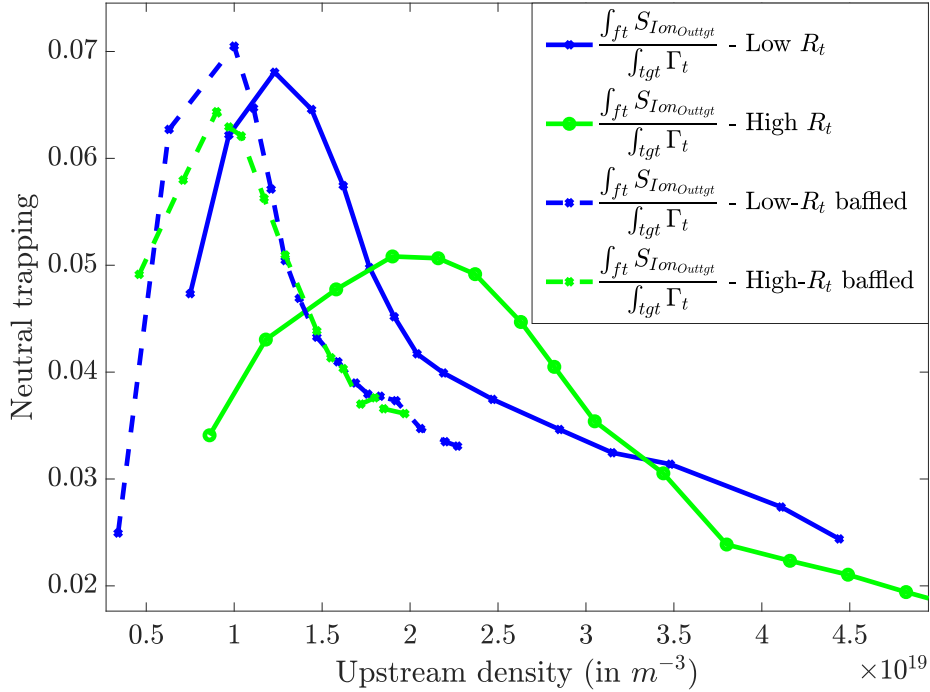
Figure 12: Measure of the neutral trapping as the fraction of neutrals which ionize in the flux tube (and not in the upstream SOL, in the core, in the Private Flux Region (PFR) or in the inner divertor). Same calculation as in Figure 10 but now with both the baffled low-R_t and baffled high-R_t.

4   Conclusions

SOLPS-ITER simulations of recent TCV experiments [15] studying the effect of total flux expansion on detachment have been performed. The experimental observations are reproduced in the modeling, i.e. a lack of total flux expansion effect on the upstream density detachment threshold, causing the configuration at low-R_t to rollover at lower upstream density than the high-R_t configuration. Analysis of the simulations show that a difference in neutral trapping between the two configurations is counteracting the effect of total flux expansion. Reducing the neutral trapping in the low-R_t configuration (by artificially tilting the TCV wall, so that both configuration have similar open divertors) allows to partially recover the total flux expansion effect. The inclusion of a baffle-like structure also allows to partially recover the total flux expansion effect by significantly increasing the neutral trapping and by homogenizing it between both configurations. The combination of both these effects allows to fully recover, and even exceed, the expected total flux expansion scaling of the detachment threshold. The importance of neutral trapping was also observed on DIII-D in [7], where deviations from the modified 2PMF were observed experimentally and in modeling, which is in line with our conclusions. Those SOLPS-ITER simulations thus confirm the importance of total flux expansion on
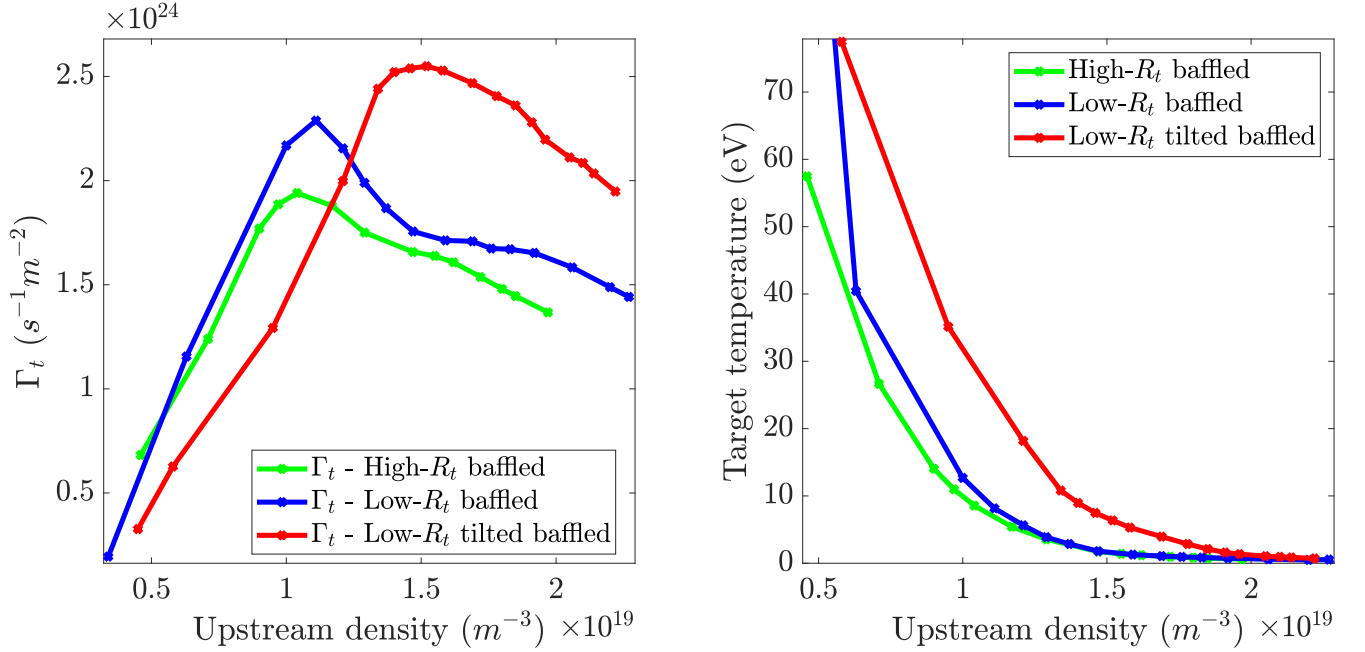
Figure 13: Evolution of the ion flux to the outer target for density scans with a baffle-like structure. Now the high-R_t baffled rolls-over at lower upstream density than the low-R_t baffled, and the ratio of detachment thresholds between the low-R_t tilted baffled and the high-R_t baffled is much closer to the total flux expansion scaling. The low-R_t tilted baffled configuration rolls-over at significantly higher upstream density than the high-R_t baffled.

the detachment threshold, but also show that the neutral trapping properties of the divertor is as important in defining the detachment threshold. In order to obtain a lower detachment threshold than in a specific configuration, one would ideally increase both the total flux expansion (increase R_t) and the neutral trapping (through baffling, changing the poloidal incidence angle).

5   Acknowledgments

References

[1] S. I. Krasheninnikov, et al., *Phys. Plasmas* **2016**, *23*, 055602.

[2] B. Lipschultz, et al., *Phys. Plasmas* **1999**, *6*, 5.

[3] A. Loarte, et al., *Nuclear Fusion* **2007**, *47*, S203.

[4] M. Wischmeier, et al., *J. Nucl. Mater.* **2015**, *463*, 22-9.

[5] A Kallenbach, et al., *Plasma Phys. Control. Fusion* **2013**, *55*, 124041.

[6] M. G. Dunne, et al., *Plasma Phys. Control. Fusion* **2017**, *59*, 014017.

[7] T.W. Petrie, et al., *Nucl. Fusion* **2013**, *53*, 113024.

[8] P. M. Valanju, et al., *Phys. Plasmas* **2009**, *16*, 056110.

[9] B. Lipschultz, et al., *Nuclear Fusion* **2016**, *56*, 056007.

[10] M. Kotschenreuther, et al., *Nuclear Fusion* **2010**, *50*, 035003.

[11] D. Moulton, et al., *Plasma Phys. Control. Fusion* **2017**, *59*, 065011.

[12] W. Morris, et al., *IEEE Trans. Plasma Sci.* **2014**.
, volume=42, pages=402,

[13] E. Havlíková, et al., *Plasma Phys. Control. Fusion* **2015**, *57*, 15001.

[14] M.V. Umansky, et al., *Physics of Plasmas* **2017**, *24*, 056112.

[15] C. Theiler, et al., *Nuclear Fusion* **2017**, *57*, 072008.

[16] X. Bonnin, et al., *Plasma Fusion Res.* **2016**, *11*, 1403102.

[17] S. Wiesen, et al., *Journal of Nuclear Materials* **2015**, *463*, 480-484.

[18] S. Coda, et al., *Nuclear Fusion* **2017**, *57*, 102011.

[19] J.-M. Moret, et al., *Fusion Eng. Des.* **2015**, *91*, 1.

[20] O. Fevrier, et al., *Rev. of Scient. Instru.* **2018**, *89*, 053502.

[21] J.R. Harrison, et al., *Nuclear Materials and Energy* **2017**, *12*, 1071-1076.

[22] J.R. Harrison, et al., *submitted to Plasma Phys. Control. Fusion* **2019**.

[23] D. Reiter, et al., *Journal of Nuclear Materials* **1992**, *196*, 80.

[24] R. C. Isler, et al., *Plasma Phys. Control. Fusion* **1994**, *36*, 171.

[25] C. K. Tsui, et al., *Phys. Plasmas* **2017**, *24*, 062508.

[26] K. Verhaegh, et al., *Nuclear Materials and Energy* **2017**, *000*.

[27] A. Fil, et al., *Contributions to Plasma Physics* **2018**.

[28] P. C. Stangeby, et al., *Nucl. Fusion* **2017**, *57*, 056007.

[29] D. Moulton, et al., *Nucl. Fusion* **2018**, *58*, 096029.

[30] M. Wensing, et al., *Plasma Physics Control. Fusion* **2019**, *submitted*.

□